한국소성가공학회 '97춘계학술대회 논문집 pp.196~206

소성예측-탄성보정에 의한 새로운 응력적분방법의 오차분석 및 적용

유 요한*, 양 동열**, 정 동택*
* 국방과학연구소 제1연구개발본부
** 한국과학기술원 기계공학과

Error Estimation of the New Stress Integration Method Using a Plastic-Predictor Followed by an Elastic-Corrector and Its Application

Y. H. Yoo, D. Y. Yang and D. T. Chung

1. Introduction

For the analysis of dynamic elastic-plastic problems, finite element program using the explicit time integration method involves the integration of, at each instant, the equations of motion to obtain the velocity gradient for each element [1]. The task of the constitutive algorithm then is to use this velocity gradient and the current values of the stress, strain, temperature, and other state variables, to calculate the corresponding incremental quantities over the time increment prescribed by the program. A very important requirement is that this task should be performed accurately and efficiently. For rate-independent elastoplasticity, most explicit finite element codes use the radial return technique. This technique was invented by Wilkins [2] and further generalized by Krieg and Key [3].

This radial return method uses an elastic-predictor followed by a plastic-corrector (EPPC method). At a given point on the current yield surface, the entire strain increment in a continuing plastic loading is first assumed to be elastic. This takes the stress point beyond the subsequent yield surface, which is then corrected through a radial return scheme to satisfy the yield condition.

Recently, a simple explicit algorithm which nearly exactly estimates the subsequent yield surface, in one time increment, with no iteration was developed by Nemat-Nasser and Chung [4]. In this technique, the entire incremental deformation over a given time increment is first regarded to be plastic, and is then corrected to account for the elastic part. In other words, the technique is based on a plastic-predictor followed by an elastic-corrector (PPEC method). This algorithm is always stable and incredibly accurate, independently of the time or strain increment. Until now, however, research result obtained by a large-scale code, in which the PPEC method has been implemented is very rare [5]. Especially, no research work has been reported for a three-dimensional problem. Although the performance of the PPEC method has been discussed by Nemat-

Nasser and Li [6], Its major weakness originates from the lack of systematic error estimation. Hence, in order to apply the PPEC method to the three-dimensional complex problems with confidence, the systematic error estimation using error map and the evaluation of simulated result in the three-dimensional problems are needed.

2. Summary of PPEC method [7]

Let τ'_{ij} be the Cauchy stress deviator with effective stress τ and orientation N_{ij},

$$\tau = \sqrt{\frac{1}{2}\tau'_{ij}\tau'_{ij}}, \qquad N_{ij} = \frac{\tau'_{ij}}{\sqrt{2}\tau}. \tag{1}$$

The total deformation rate tensor is given by

$$D_{ij} = D_{ij}^{e} + D_{ij}^{p} \tag{2}$$

where D_{ij}^{e} and D_{ij}^{p} (deviatoric without a prime) are the elastic and the plastic deformation rate tensor, respectively. The elasticity is given by

$$\overset{o}{\tau} = C_{ijkl}D_{kl}^{e}, \tag{3}$$

and the plasticity is defined by

$$D_{ij}^{p} = \dot{\gamma}N_{ij}, \ \dot{\gamma} = \sqrt{D_{ij}^{p}D_{ij}^{p}}, \tag{4}$$

where C_{ijkl} is the elasticity tensor, $\dot{\gamma}$ is the plastic strain rate, and the objective stress rate $\overset{o}{\tau}_{ij}$ is defined by

$$\overset{o}{\tau}_{ij} = \dot{\tau}_{ij} - W_{ik}\tau_{kj} + \tau_{ik}W_{kj}, \tag{5}$$

where W_{ij} is the spin tensor.

Let τ be defined by a flow rule of the form

$$\tau = g(\dot{\gamma}, \gamma, T), \tag{6}$$

$$\gamma = \int_0^t \dot{\gamma}(\xi)d\xi, \ \gamma_{eff} \equiv \sqrt{2}\gamma, \tag{7}$$

where γ_{eff} is the effective plastic strain.

For simplicity, assume elastic isotropy and use equations (2)-(4) to obtain

$$\overset{o}{\tau}'_{ij} = 2G(D'_{ij} - D_{ij}^{p}) = 2G(D'_{ij} - \dot{\gamma}N_{ij}). \tag{8}$$

It can be shown by simple manipulation [6] that the basic constitutive equations are reduced to a tensor relation for $\dot{\tau}'_{ij}$, and a scalar relation for $\dot{\tau}$, as follows.

$$\dot{\tau}'_{ij} = 2GD'_{ij} - 2G\dot{\gamma}N_{ij} + \left\{W_{ik}\tau'_{kj} - \tau'_{ik}W_{kj}\right\}, \tag{9}$$

$$\frac{\dot{\tau}}{\sqrt{2}G} + \dot{\gamma} = d, \ d = N_{ij}D'_{ij} \tag{10}$$

The following is the numerical algorithm of the PPEC method.

Step 1. Solve the following set of constitutive equations :

$$\dot{\tau}'_{ij} = 2GD'_{ij} - 2G\dot{\gamma}N_{ij} + \left\{W_{ik}\tau'_{kj} - \tau'_{ik}W_{kj}\right\},\ \frac{\dot{\tau}}{\sqrt{2}G} + \dot{\gamma} = d,\ d = N_{ij}D'_{ij}.$$

Step 2. Integrate the tensor equation twice from time t to t+ ϑ (first $\vartheta = \Delta t/2$, then $\vartheta = \Delta t$) to solve for $\tau'^{p}_{ij}(t+\Delta t/2)$ and $\tau'^{p}_{ij}(t+\Delta t)$, respectively [8]:

$$\begin{aligned}&\tau'^{p}_{ij}(t+\vartheta) + \xi_0\left\{\tau'^{p}_{ik}(t+\vartheta)W_{kj} - W_{ik}\tau'^{p}_{kj}(t+\vartheta)\right\}\\ &\quad = \zeta_0\left[\tau'_{ij}(t) + \xi'_0\left\{\tau'_{ik}(t)W_{kj} - W_{ik}\tau'_{kj}(t)\right\}\right] + \eta_0 D'_{ij}.\end{aligned} \tag{11}$$

Step 3. Find the orientation of the stress tensors at time t+$\Delta t/2$ and t+Δt, respectively :

$$N_{ij}(t+\Delta t/2) \equiv \frac{\tau'^{p}_{ij}(t+\Delta t/2)}{\left|\tau'^{p}_{ij}(t+\Delta t/2)\right|},\ N_{ij}(t+\Delta t) \equiv \frac{\tau'^{p}_{ij}(t+\Delta t)}{\left|\tau'^{p}_{ij}(t+\Delta t)\right|}. \tag{12}$$

Step 4. Find d* with one Gauss integration points as follows :

$$d^* = N_{ij}(t+\Delta t/2)D'_{ij}. \tag{13}$$

Step 5. Integrate the scalar equation to find the effective stress and plastic strain increment as follows :

$$\tau(t+\Delta t) = \frac{\tau^a(t+\Delta t) + \eta(t+\Delta t)\tau(t)}{1+\eta(t+\Delta t)}, \tag{14}$$

$$\Delta\gamma = \left(d^* - \dot{\gamma}^*_{er}\right)\Delta t = d^*\Delta t - \frac{\tau^a(t+\Delta t) - \tau(t)}{\sqrt{2}G\left(1+\eta(t+\Delta t)\right)}, \tag{15}$$

where

$$\tau^a(t+\Delta t) = g\left(d^*,\ \gamma(t) + d^*\Delta t,\ T^a(t+\Delta t)\right), \tag{16}$$

$$\eta(t+\Delta t) = \frac{1}{\sqrt{2}GA^*}\left(\frac{\partial g}{\partial\dot{\gamma}}\frac{1}{\Delta t} + \frac{\partial g}{\partial\gamma} + \frac{\partial g}{\partial T}\frac{\chi}{\rho C_v}\tau^*\right), \tag{17}$$

$$\dot{\gamma}^*_{er} = \frac{\tau^a(t+\Delta t) - \tau(t)}{\sqrt{2}G\left\{1+\eta(t+\Delta t)\right\}\Delta t}. \tag{18}$$

If $\Delta\gamma > 0$, go to step 6, otherwise go to step 7.

Step 6. Normalize the stress tensor :

$$\tau'_{ij}(t+\Delta t) = \sqrt{2}\tau(t+\Delta t)N_{ij}(t+\Delta t). \tag{19}$$

Go to step 2 for the next time step calculation.

Step 7. Integrate the tensor equation with $D_{ij}{}^{p} = 0$ and solve for $\tau'_{ij}(t+\Delta t)$:

$$\tau'_{ij}(t+\Delta t)+\frac{\Delta t}{2}\left\{\tau'_{ik}(t+\Delta t)W_{kj}-W_{ik}\tau'_{kj}(t+\Delta t)\right\}= \tau'_{ij}(t)-\frac{\Delta t}{2}\left\{\tau'_{ik}(t)W_{kj}-W_{ik}\tau'_{kj}(t)\right\}+2G\Delta tD'_{ij}. \quad (20)$$

Go to step 2 for the next time step calculation.

3. Application to the Johnson-Cook model

In the Johnson-Cook model [9], the von Mises flow stress, $\bar{\sigma}$, is expressed as

$$\bar{\sigma}=\left[A+B\bar{\varepsilon}^{n}\right]\cdot\left[1+C\ln\left(\frac{\dot{\bar{\varepsilon}}}{\dot{\bar{\varepsilon}}_0}\right)\right]\cdot\left[1-\left(\frac{T-T_r}{T_m-T_r}\right)^{m}\right] \quad (21)$$

$$\bar{\sigma}=\sqrt{\frac{3}{2}\sigma'_{ij}\sigma'_{ij}}, \quad (22)$$

$$\dot{\bar{\varepsilon}}=\sqrt{\frac{2}{3}D^{p}_{ij}D^{p}_{ij}}, \quad \bar{\varepsilon}=\int_0^t\dot{\bar{\varepsilon}}(\xi)d\xi \quad (23)$$

where $\bar{\varepsilon}$ and $\dot{\bar{\varepsilon}}$ are the equivalent plastic strain and the equivalent plastic strain rate, $\dot{\bar{\varepsilon}}_0$ is a constant, and T, T_m and T_r are current, melting and reference temperatures, respectively. A, B, C, n and m are material constants. The expression in the first set of brackets represents the effect of strain hardening. The expressions in the second and third sets of brackets represent the effects of strain rate hardening and temperature softening, respectively.

The temperature increase, ΔT , by adiabatic heating is expressed as

$$\Delta T=\int_0^t\frac{\chi}{\rho C_v}\bar{\sigma}\,\dot{\bar{\varepsilon}}\,dt \quad (24)$$

where C_v is the constant-volume heat capacity of the material, and χ defines the fraction of the plastic work which is used to increase the material temperature [10]. The summation of the temperature of the current time step and yields the temperature of the next time step which makes an influence upon the flow stress of the next time step.

In the Johnson-Cook model, τ in equation (6) and η in equation (17) are derived as follows :

$$\tau(\dot{\gamma},\gamma,T)=\left[A'+B'\gamma^{n}\right]\cdot\left[1+C\ln\left(\frac{\dot{\gamma}}{\dot{\gamma}_0}\right)\right]\cdot\left[1-\left(\frac{T-T_r}{T_m-T_r}\right)^{m}\right] \quad (25)$$

$$\eta(t+\Delta t)=\frac{\tau^a(t+\Delta t)}{\sqrt{2}GA^*}\left[\frac{C}{\left\{1+C\ln\left(\frac{d^*}{\dot\gamma_0}\right)\right\}d^*\Delta t}+\frac{Bn\left\{\gamma(t)+d^*\Delta t\right\}^{n-1}}{A+B\left\{\gamma(t)+d^*\Delta t\right\}^n}\right.$$
$$\left.-\frac{\chi\tau^* m\left\{T^a(t+\Delta t)-T_r\right\}^{m-1}}{\rho C_v\left\{(T_m-T_r)^m-\left(T^a(t+\Delta t)-T_r\right)^m\right\}}\right] \tag{26}$$

$$A^*=1+\frac{m\theta\chi\tau^a(t+\Delta t)d^*\Delta t\left\{T^a(t+\Delta t)-T_r\right\}^{m-1}}{\rho C_v\left\{(T_m-T_r)^m-\left(T^a(t+\Delta t)-T_r\right)^m\right\}} \tag{27}$$

where material constants A and B of equation (21) are related to A′ and B′ of equation (25) by the following equations.

$$A'=\frac{A}{\sqrt{3}},\quad B'=\frac{B}{\sqrt{3}}\left(\sqrt{\frac{2}{3}}\right)^n \tag{28}$$

4. Error estimation

First, in order to check proper implementation of the PPEC algorithm and elastic-plastic response under large strain and rotation, the following velocity gradients are considered :

$$L_1=\begin{pmatrix}20s^{-1} & 0 & 0\\ 2s^{-1} & -10s^{-1} & 0\\ 0 & 0 & -10s^{-1}\end{pmatrix},\quad \text{for } 0\le t\le 500\mu s, \tag{29}$$

$$L_2=\begin{pmatrix}20s^{-1} & 3000s^{-1} & 0\\ -3000s^{-1} & 20s^{-1} & 0\\ 0 & 0 & 0\end{pmatrix},\quad \text{for } 500< t\le 1000\mu s. \tag{30}$$

In the computation, AISI 4340 steel with the Johnson-Cook yield surface model is used. The shear modulus G = 80.8 GPa and the Poisson's ratio ν = 0.3 are used, with the initial temperature $T_i = 950^oC$, and other material properties for AISI 4340 steel are the same as the published experimental data [9].

The PPEC method with 10 time steps is used to obtain the solution, and then the EPPC method with 10 and 10000 time steps is used to compare this result with the solution obtained by the PPEC method. Figs. 1(a)-(c) show the time plots of the stress components. The result of 10000 increments of the EPPC method is essentially an exact solution. The result of 10 increments of the PPEC method is the same as the result of 10000 increments of the EPPC method, even though a large rotation accompanies the

deformation. However, the result of 10 increments of the EPPC method does not produce the accurate consequence.

Next, attention is focused on an assessment of accuracy under various initial stress states. For this purpose, iso-error maps are employed. This method has been used in the previous research works [11-13]. Iso-error maps corresponding to specified loading increments provide a systematic approach to test the accuracy of algorithms for elastoplasticity.

Three points on the yield surface with σ_3=0 are selected which are representative of a wide range of possible states of stress. These points, A, B and C and shown in Fig. 2, correspond to uniaxial, biaxial and pure shear stress states, respectively. The stresses corresponding to the states of strain predefined are then computed by applying the algorithm. Computed results are reported in terms of the relative root mean square of the error between the exact solution and the computation, which is obtained according to the expression

$$\delta(\%) = \frac{\sqrt{\left(\sigma_{ij} - \sigma^*_{ij}\right)\left(\sigma_{ij} - \sigma^*_{ij}\right)}}{\sqrt{\sigma^*_{ij}\ \sigma^*_{ij}}} \times 100 \qquad (31)$$

where, σ_{ij} is the result obtained by applying the algorithm, whereas σ^*_{ij} is the exact solution corresponding to the specified strain increment. The exact solution is obtained for any given strain increment by repeated application of the EPPC method with 10000 subincrements.

The iso-error maps corresponding to points A, B and C are shown in Figs. 3-5. The computational condition is the same as the previous one except for $B = C = \chi = 0$. Then, elastic-perfectly plastic material property with the initial yield stress is assumed. The results of the EPPC method show the tendency of increasing error with increasing strain increment size, whereas the results of the PPEC method maintain constant error level irrelevant to strain increment size. In the EPPC method, a relatively good accuracy (within 8.0 %) is obtained for moderate strain increment size, on the other hand, very accurate results (within 0.005 %) is obtained in the PPEC method. For more clear understanding, the computed results of the EPPC and the PPEC methods are shown in Figs. 6 and 7 with different definition of axes. It is noted that the level of error obtained from the PPEC method is more accurate by two or three orders of magnitude than the EPPC method. From these results, it may be concluded that the employment of the PPEC method is indispensable for better outcome in elastic-plastic analysis.

5. Application to buckling problem

The computed results corresponding to the numerical simulation of buckling problem are presented below. The main objective of the simulation is to compare the computed results of the EPPC and PPEC methods in three-dimensional problems.

The geometry and finite element mesh considered for the buckling problem are shown in Fig. 8. The computation is performed by imposing uniform velocity of 0.1 mm/μs on the upper die. From obvious symmetry considerations, only one-half of the

specimen need be analyzed. A total of 111 eight-node isoparametric hexahedrons are used in the computation. AISI 4340 steel with the Johnson-Cook yield surface model is chosen for a specimen material. The material constants and computation conditions are the same as the first example of section 4 except that the initial temperature T_i is 10^oC. The coefficient of friction is chosen as 0.2. The buckling problem is solved using the prescribed uniform velocity on the upper die during 250 μs. The resulting deformation pattern for the specimen is shown in Fig. 9. For the sake of comparison between the EPPC and the PPEC, the distributions of equivalent plastic strains and stresses obtained from the two methods are illustrated together in Figs. 10 and 11. Note that the substantial difference between the EPPC and the PPEC results is observed in the distributions of stresses and equivalent plastic strain. These results demonstrate that the stress integration using the PPEC method is necessary so as to obtain the accurate values of stresses and strain.

References

[1] Y. H. Yoo, D. Y. Yang, 1997, Finite element modelling of high-velocity impact forging process by the explicit time integration method, Journal of Materials Processing Technology, Vol. 63, pp. 718~723.

[2] M. Wilkins, 1964, Calculation of elastic-plastic flow, Methods in Computational Physics, Vol. 3, Academic Press, New York, pp. 211-263.

[3] R. D. Kreig and S. W. Key, 1976, Implementation of a time dependent plasticity theory into structural computer programs, Vol. 20 of Constitutive Equations in Viscoplasticity: Computational and Engineering Aspects, ASME, New York, pp. 125-137.

[4] S. Nemat-Nasser and D. T. Chung, 1992, An explicit constitutive algorithm for large-strain rate elastic-viscoplasticity, Comput. Methods Appl. Mech. Eng., Vol. 95, pp. 205-219.

[5] S. Nemat-Nasser, Y. F. Li and J. B. Isaacs, 1994, Experimental/computational evaluation of flow stress at high strain rates with application to adiabatic shear banding, Mechanics of Materials, Vol. 17, pp. 111-134.

[6] S. Nemat-Nasser and Y. F. Li, 1992, A new explicit algorithm for finite-deformation elastoplasticity and viscoelastoplasticity: Performance evaluation, Comput. Struct., Vol. 44, pp. 937-963.

[7] S. Nemat-Nasserand Y. F. Li, 1994, An algorithm for large-scale computational finite-deformation plasticity, Mechanics of Materials, Vol. 18, pp. 231-264.

[8] S. Nemat-Nasser, 1991, Rate-independent finite-deformation elastoplasticity: A new explicit constitutive algorithm, Mechanics of Materials, Vol. 11, pp. 235-249.

[9] G. R. Johnson and W. H. Cook, 1983, A constitutive model and data for metals subjected to large strain rates and high temperature, Proc. of 7th Int. Symp. on Ballistics, pp. 541-547.

[10] J. J. Mason, A. J. Rosakis and G. Ravichandran, 1994, On the strain and strain rate dependence of the fraction of plastic work converted to heat : an experimental study using high speed infrared detectors and the Kolsky bar, Mechanics of Materials,

Vol. 17, pp. 135-145.

[11] R. D. Krieg and D. B. Krieg, 1977, Accuracies of numerical solution methods for the elastic-perfectly plastic model, J. Pressure Vessel Tech., ASME, Vol. 99, pp. 510-515.

[12] H. L. Schreyer, R. L. Kulak and J. M. Kramer, 1979, Accurate numerical solution for elastic-plastic models, J. Pressure Vessel Tech., ASME, Vol. 101, pp. 226-234.

[13] J. C. Simo and R. L. Taylor, 1986, A return mapping algorithm for plane stress elastoplasticity, Internat. J. Numer. Methods Engrg., Vol. 22, pp. 649-670.

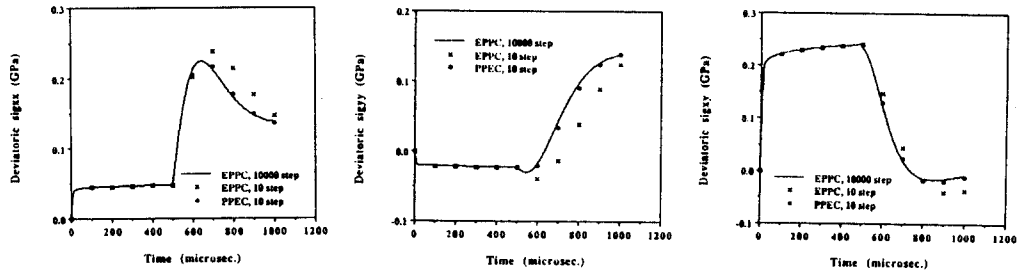

Fig. 1 Performance demonstration of the PPEC method with the Johnson-Cook model; (a) time history of stress σ_{xx}, (b) time history of stress σ_{yy}, (c) time history of stress σ_{xy}

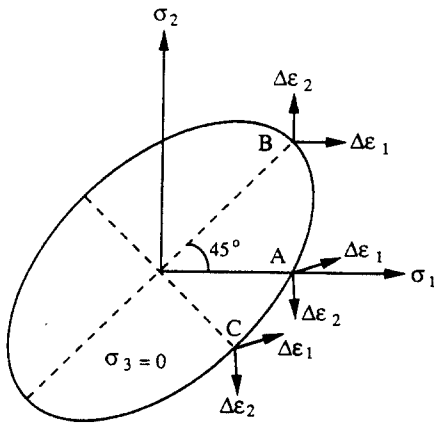

Fig. 2 Yield surface with principal stress σ_3=0; points for iso-error maps

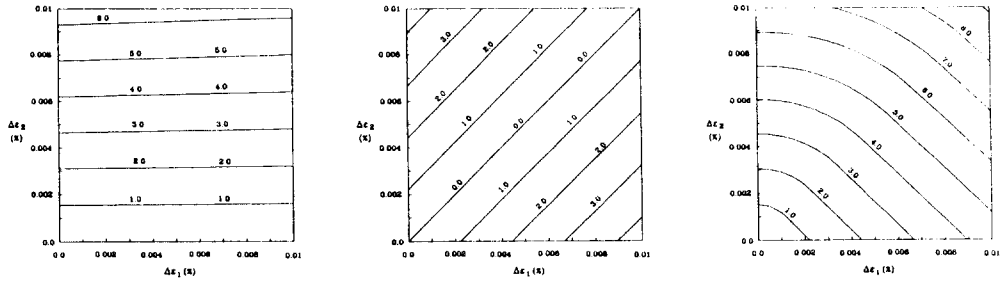

(a) (b) (c)

Fig. 3 Iso-error maps obtained from the EPPC method; (a) point A, (b) point B, (c) point C

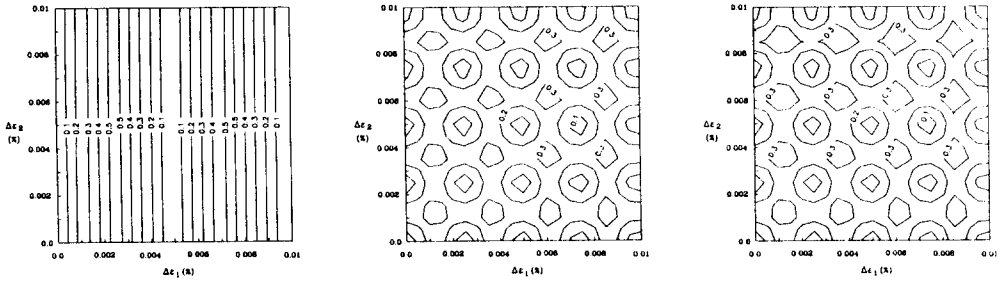

(a) (b) (c)

Fig. 4 Iso-error maps obtained from the PPEC method (contour values : $\delta X10^2$); (a) point A, (b) point B, (c) point C

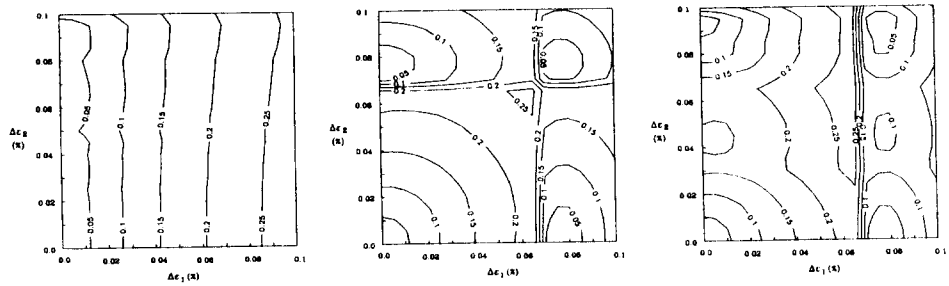

(a) (b) (c)

Fig. 5 Iso-error maps obtained from the PPEC method in the case of large strain increment (contour values : $\delta X10^2$); (a) point A, (b) point B, (c) point C

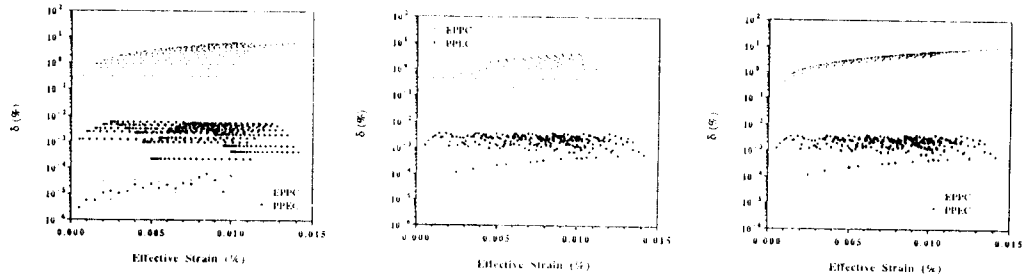

(a) (b) (c)

Fig. 6 Comparison of error between the EPPC and the PPEC methods; (a) point A, (b) point B, (c) point C

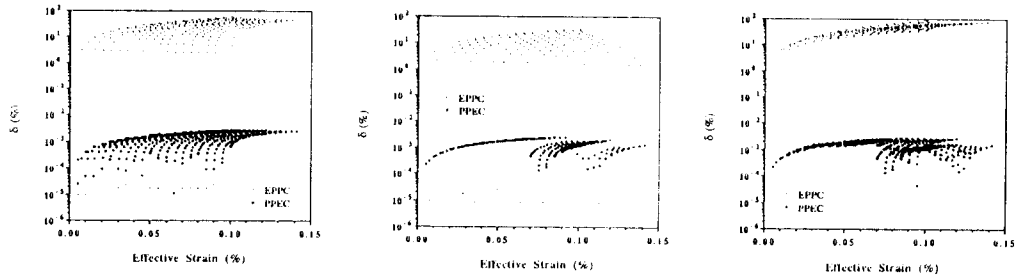

(a) (b) (c)

Fig. 7 Comparison of error between the EPPC and the PPEC methods in the case of large strain increment; (a) point A, (b) point B, (c) point C

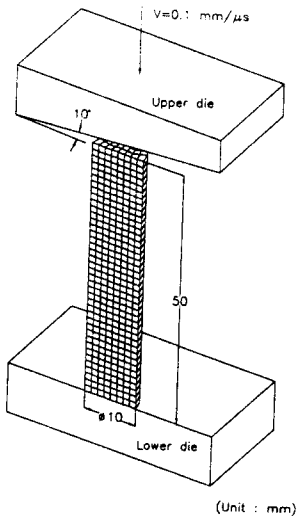

Fig. 8 Dimensions and finite element meshes for the buckling problem

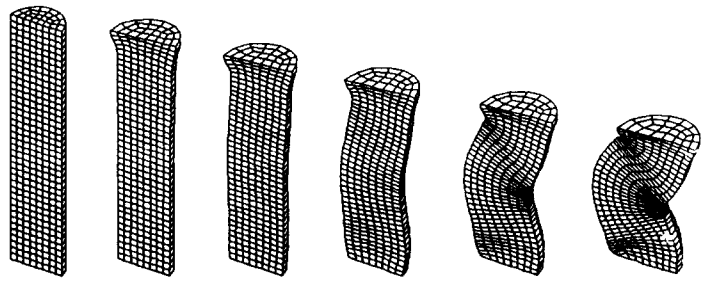

* at 0 μs * at 50 μs * at 100 μs * at 150 μs * at 200 μs * at 250 μs

Fig. 9 Deformation sequence of the specimen in the buckling analysis

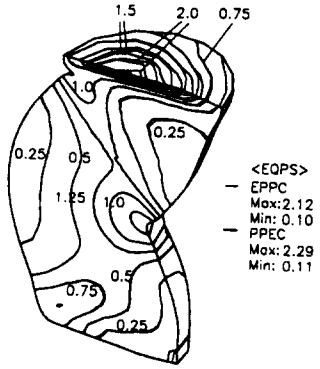

Fig. 10 Comparison of equivalent plastic strain distribution between the EPPC and the PPEC methods at the final stage in the buckling analysis

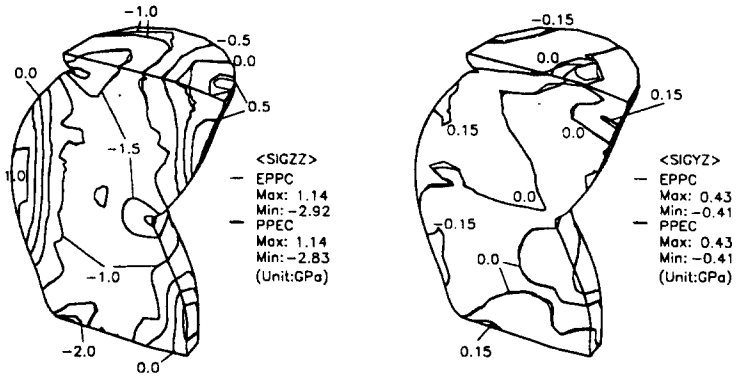

(a) (b)

Fig. 11 Comparison of stress distributions between the EPPC and the PPEC methods at the final stage in the buckling analysis; (a) stress σ_{zz}, (b) stress σ_{yz}